

Lawrence Berkeley National Laboratory

Recent Work

Title

TRACER SURFACE DIFFUSION ON UO₂

Permalink

<https://escholarship.org/uc/item/9bq6h5r4>

Authors

Zhou, S.Y.

Olander, D.R.

Publication Date

1983-05-01



Lawrence Berkeley Laboratory

UNIVERSITY OF CALIFORNIA

Materials & Molecular Research Division

RECEIVED
LAWRENCE
BERKELEY LABORATORY
JUN 8 1983
LIBRARY AND
DOCUMENTS SECTION

To be submitted for publication

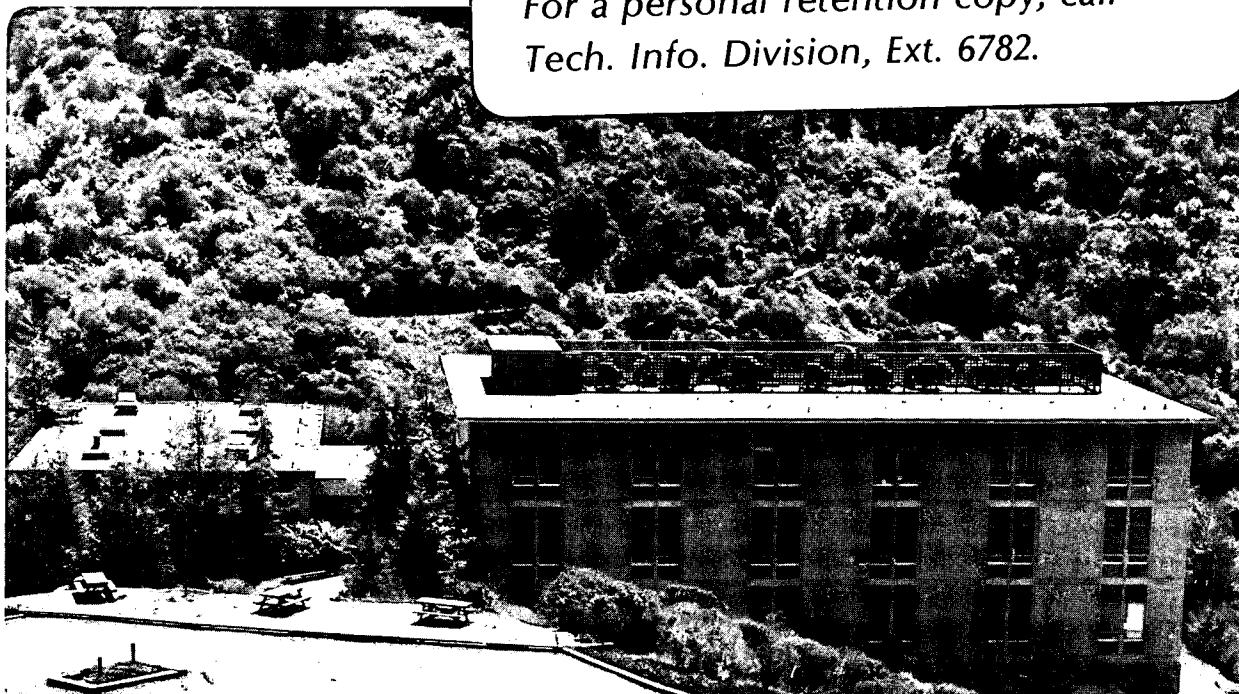
TRACER SURFACE DIFFUSION ON UO_2

S.Y. Zhou and D.R. Olander

May 1983

TWO-WEEK LOAN COPY

*This is a Library Circulating Copy
which may be borrowed for two weeks.
For a personal retention copy, call
Tech. Info. Division, Ext. 6782.*



LBL-16070
e.2

DISCLAIMER

This document was prepared as an account of work sponsored by the United States Government. While this document is believed to contain correct information, neither the United States Government nor any agency thereof, nor the Regents of the University of California, nor any of their employees, makes any warranty, express or implied, or assumes any legal responsibility for the accuracy, completeness, or usefulness of any information, apparatus, product, or process disclosed, or represents that its use would not infringe privately owned rights. Reference herein to any specific commercial product, process, or service by its trade name, trademark, manufacturer, or otherwise, does not necessarily constitute or imply its endorsement, recommendation, or favoring by the United States Government or any agency thereof, or the Regents of the University of California. The views and opinions of authors expressed herein do not necessarily state or reflect those of the United States Government or any agency thereof or the Regents of the University of California.

TRACER SURFACE DIFFUSION ON UO_2

by

S.Y. Zhou* and D.R. Olander

Materials and Molecular Research Division of the Lawrence Berkeley
Laboratory and the Department of Nuclear Engineering of the University
of California, Berkeley, California, U. S. A. 94720

* Current address: Institute of Atomic Energy, Academia Sinica,
Beijing, PRC

ABSTRACT

Surface diffusion on UO_2 was measured by the spreading of U-234 tracer on the surface of a duplex diffusion couple consisting of wafers of depleted and enriched UO_2 joined by a bond of uranium metal. Spurious gas phase transport was eliminated by a masking technique. Surface diffusion coefficients measured at temperature between 1760 and 2110°C ranged from 0.1 to 2 cm^2/s . These results correspond to Arrhenius-type behavior with an activation energy of 72 ± 15 kcal/mole and a preexponential factor 5×10^6 cm^2/s with a 1-2 order of magnitudes uncertainty range. The preexponential factor was in reasonable accord with the nonlocalized surface diffusion model of Bonzel, although the jump distance implicit in this theory appears to be unacceptably large. No significant effect of the atomic weight of the inert species in the gaseous environment at 1 atm pressure was detected, a result which is not inconsistent with the theory.

INTRODUCTION

Mass transport methods such as scratch decay and grain boundary grooving are responsible for nearly all of the data on surface self diffusion on UO_2 (1-5). The data obtained by Marlowe and Kaznoff (6) using a tracer technique have been claimed to be in good agreement with the results of mass transport experiments (4,5). However, Robertson(7) first pointed out that correct interpretation of the data of Marlowe and Kaznoff to account for simultaneous volume and surface diffusion during tracer spreading results in much larger surface diffusivities than originally reported by these authors. Each improvement in the mathematical treatment of the tracer spreading problem (8, 9, 10) resulted in larger deduced values of surface diffusivity, until now the discrepancy between the mass transport and tracer results at 1900°C stands between three and four orders of magnitude. Although the surface diffusion coefficients from several different mass transport experiments are quite consistent, Matzke (11) was unable to perform such an experiment on single crystal specimens because of the development of striations on the surface which grew rather than diminished with annealing time.

Surface mobility may not be a unique property of the solid. The possibility that surface diffusion on UO_2 might depend upon collision between UO_2 molecules migrating on the surface and atoms impinging from the gas phase has been suggested independently by Buescher and Meyer(12) and by Mikhlin (13). This notion has been further developed by Nixon and MacInnes (14). Variation of the gaseous atmosphere during the diffusion anneal may help elucidate this feature of the process.

For accurate results, a tracer surface diffusion experiment should incorporate the following features.

- A masking technique to protect the surfaces from evaporation or spurious transport of tracer by molecular diffusion in the gas. The later parasitic transport process was shown to be very significant in the work of Furuya and Koizumi (15).
- A simple geometry of the diffusion couple to permit accurate analysis of the data to yield the surface diffusion coefficient.
- A method of reducing the solid-solid contact resistance between enriched and depleted parts of the diffusion couple.
- Avoidance of pure hydrogen or strongly oxidizing gases in contact with the solid during the anneal. Such environments can alter the oxide stoichiometry and thereby affect the uranium volume diffusion coefficient on which data interpretation depends.
- Use of isotopically enriched and depleted uranium in the oxide diffusion couple, with U-234 as the actual tracer. Use of plutonium as a "chemical tracer", as in the experiments of Furuya and Kozumi (15), risks gas transfer of the heavy metals between the source and sink components of the couple, as has been demonstrated by Matzke and Lambert (16).

The diffusion couple consisted of two wafers of UO_2 , one of which was enriched to 93% U-235 and the other depleted to 0.2% U-235. The two wafers were bonded together so that surface exchange of uranium isotopes across the wafer-wafer interface was reasonably efficient. Isotope exchange across the interior portion of the interface by volume diffusion also occurred, but very slowly compared to exchange by surface

diffusion. When heated, uranium isotopes transferred between the two wafers but no net uranium flow took place. The face of the enriched wafer lost the light isotopes by volume diffusional exchange with U-238 supplied by the depleted wafer. The reverse process occurred on the face of the depleted wafer. Transport of the uranium isotope was along the surface, but storage of the tracer in quantities sufficient to measure by detection of the alpha particles emitted by U-234 required diffusion into the solid from the surfaces. Even though an interface resistance arising from imperfect joining of the two wafers was present, the symmetry of the duplex specimen streamlined the mathematical analysis of the coupled surface and volume diffusion model of tracer spreading. These processes led to radial distribution of the alpha radioactivity along both faces of the specimen following an anneal. Because the bulk of the initially depleted wafer contained little U-234, radial spreading of the tracer was most accurately determined by measurement of this face. The comparable reduction in tracer concentration in the enriched wafer was difficult to detect because of the high background radioactivity from the bulk of this material.

EXPERIMENTAL

Each UO_2 wafer was 1 mm thick and 15 mm in diameter. The enriched and depleted wafers were sintered together with the aid of a thin uranium metal foil placed between them. Annealing at 1500°C for 1 hour in an atmosphere of hydrogen saturated with water vapor at 23°C sufficed to produce a good bond over most of the interface. Sintering with the uranium bond was not possible in dry hydrogen or in vacuum.

Due to contraction of the liquid uranium into the void space between the two wafers and the lack of wetting of the oxide by the metal, the periphery of the interface between the two wafers was not completely bonded. This introduced a contact resistance into the transport process which had to be accounted for in the data analysis. The metallic uranium reacted with water from the moist hydrogen and was converted to oxide at the interface. A single specimen was used for all experiments.

Following the activity distribution measurement after each anneal, the enriched and depleted faces of the duplex specimen were ground to a mirror finish with abrasives. Sufficient material ($\sim 10 \mu\text{m}$) was removed in this process to return the alpha radioactivity of each face to the value characteristic of the original materials. The duplex specimen was cleaned ultrasonically in methanol and loaded into the rig shown in Fig. 1, which was then heated in a tungsten resistance furnace. Holes in bottom of the crucible permitted access of the slowly-flowing gas to the specimen. A key feature of the apparatus was the rhenium foils ($25 \mu\text{m}$ thick) which covered both faces of the specimen. These were designed to eliminate UO_2 vaporization and vapor transport of the tracer during the anneals. There was essentially no gap between the foils and the specimen faces; the foils adhered to the UO_2 faces but could be peeled off following an experiment.

In conducting an anneal, the system was first heated to $\sim 1000^\circ\text{C}$ for about 10 minutes for degassing and then the temperature was quickly raised to the desired value. The anneals ranged in duration from 2 hours

at 1760°C to 15 minutes at 2100°C. In the set of experiments covering this temperature range, the gas contacting the specimen was hydrogen saturated with water at 23°C. In a second set of experiments, the temperature was fixed at 1815°C and anneals were conducted in atmospheres of xenon, krypton, argon and helium at 1 atm. Finally, one experiment in vacuum was performed.

Following each anneal, the radial distribution of alpha activity on the depleted face of the duplex specimen was measured using the aperture technique of Marlowe and Kaznoff (6). The enriched face and the specimen sides were covered with scotch tape, which sufficed to block all alpha particles from these surfaces from contributing to the count rate. The depleted face was partially covered with one of a series of brass disks 75 μm thick with apertures diameters ranging from 3 mm to 14 mm. The alpha radioactivity of the uncovered portion of the sample surface was measured in a gas flow proportional counter. The activities of the enriched and depleted faces (following polishing to remove the activity distributions caused by previous anneal) were measured in the same counter.

DATA REDUCTION

For use of the theory, the aperture count rate data had to be deconvoluted to provide a measure of the local flux of alpha particles leaving a unit area of surface as a function of radial position on the initially depleted surface. The quantity provided by the theory is the dimensionless countrate:

$$R = \frac{I - I_d}{I_e - I_d} \quad (1)$$

where I is the current of alpha particles leaving the surface at radius r and the quantities I_e and I_d are the comparable currents from the surfaces of the original enriched and depleted materials, respectively.

The countrates measured with an aperture of radius r are integrals of the currents:

$$J(r) = 2\pi \int_0^r I(r') r' dr' \quad (2)$$

To deduce $I(r)$ from the 8 or 9 measurements of $J(r)$, the former was assumed to be represented by the polynomial:

$$I(r) = A_0 + A_2 r^2 + A_3 r^3 \quad (3)$$

Because the activity distribution must exhibit a minimum at the origin, no linear term is included in Eq(3) and in addition, the parameter A_2 must be positive. Inserting Eq(3) into Eq(2) yields the equation to which the radioactivity measurements were fitted:

$$J(r) = 2\pi \left(\frac{1}{2} A_0 r^2 + \frac{1}{4} A_2 r^4 + \frac{1}{5} A_3 r^5 \right) \quad (4)$$

If the fitting procedure produced a negative value of A_2 , this parameter was set equal to zero and the data fitted to the two-parameter polynomial involving only the constants A_0 and A_3 . Once the coefficients had been determined from the data, the dimensionless countrate given by Eq (1) was computed as a function of radial position. Values of I_e and I_d were measured prior to each anneal, but only small variations from similar measurements for previous experiments were noted.

The results of all experiments are shown in Table 1. The runs

are numbered in the order that the tests were conducted. This may be significant because the same duplex specimen was used for all experiments. The fourth row indicates that the gaseous environment was wet hydrogen for the 8 experiments in which temperature was varied. The remaining runs were at the same temperature but used different ambient gases. The initial sample radius was 7.3 mm. Following run no. 6, the sample was remeasured and found to have been reduced by 0.8 mm in diameter due to the grinding operation used to prepare the specimen for each new run. The radii of the apertures used to mask portions of the depleted wafer surface during alpha counting are listed in the first column of Table 1. The counts recorded in 8 minutes from each aperture (which are the values of J in Eq (4)) are listed in the remainder of the table.

TRACER SPREADING MODEL

In addition to azimuthal symmetry, the geometry of the duplex specimen is symmetric about the midplane. Thus, only the depleted half, which consisted of a cylindrical side of height l and radius a and a circular surface of the same radius, needs to be treated. Because the wafers are thin ($a/l = 7$), the two-region geometry can be approximated by a single circular region of the same area as the actual surface. The equivalent radius is:

$$a_{\text{eff}}^2 = a^2 + 2al \quad (5)$$

The tracer atom balance on this surface is:

$$\frac{\partial C_s^+}{\partial t} = D_s \frac{1}{r} \frac{\partial}{\partial r} \left(r \frac{\partial C_s^+}{\partial r} \right) + D_v \left(\frac{\partial C_v^+}{\partial z} \right)_{z=0} \quad (6)$$

where C_s^+ is the tracer surface concentration (atoms per unit area) at radial location r and C_v is the bulk tracer concentration (atoms per unit volume) at radial position r and penetration depth z . D_s and D_v are the surface and bulk diffusion coefficients of uranium on or in UO_2 . Since the specimen was polycrystalline, the latter reflects contributions from lattice and grain boundary diffusion. Because of the masking technique described earlier, both surface evaporation and tracer vapor transport are neglected in Eq(6).

The location $r = a_{eff}$ is the periphery of the interface between the enriched and depleted wafers. Because this joint is imperfect, the boundary condition here assumes transport across the interface to be determined by an interface conductance h according to the equation:

$$D_s \left(\frac{\partial C_s^+}{\partial r} \right)_{r=a_{eff}} = h \left[(C_s^+)_m - (C_s^+)_{r=a_{eff}} \right] \quad (7)$$

where $(C_s^+)_m$ is the hypothetical surface concentration in the midplane of the specimen periphery and $(C_s^+)_{r=a_{eff}}$ is the actual tracer surface concentration on the depleted wafer side of this interface.

The dimensionless surface tracer concentration is defined by:

$$u = \frac{C_s^+ / C_s - q_d}{q_e - q_d} \quad (8)$$

where C_s is the number of atoms of uranium per unit area of the UO_2 surface and q_e and q_d are the U-235 fractions of the enriched and depleted wafers, respectively.

The comparable dimensionless bulk tracer concentration is:

$$v = \frac{C_v^+ / C_v - q_d}{q_e - q_d} \quad (9)$$

where C_v is the number of uranium atoms per unit volume in UO_2 .

Radial position is nondimensionalized by the effective radius of the specimen:

$$\eta = r/a_{\text{eff}} \quad (10)$$

Penetration depth is expressed in terms of the alpha particle range in UO_2 , z_F :

$$Z = z/z_F \quad (11)$$

and the dimensionless time is:

$$\tau = D_v t / z_F^2 \quad (12)$$

The dimensionless form of Eq(6) is:

$$EG \frac{\partial u}{\partial \tau} = \frac{1}{\eta} \frac{\partial}{\partial \eta} \left(\eta \frac{\partial u}{\partial \eta} \right) + \sqrt{\tau} E \left(\frac{\partial v}{\partial Z} \right)_{Z=0} \quad (13)$$

where

$$E = \frac{a_{\text{eff}}^2 D_v C_v}{\sqrt{\pi} z_F D_s C_s} \quad (14)$$

$$G = \frac{\sqrt{\pi} C_s}{z_F C_v} \quad (15)$$

The parameter G consists of known physical properties and is equal to 5×10^{-5} .

Fick's second law for tracer diffusion in the bulk is:

$$\frac{\partial v}{\partial \tau} = \frac{\partial^2 v}{\partial z^2} \quad (16)$$

for which the initial condition (for the depleted face to the specimen) is

$$v(z, 0) = 0 \quad (17)$$

and the boundary conditions are:

$$v(0, \tau) = u(\eta, \tau) \quad (18)$$

and

$$v(\infty, \tau) = 0 \quad (19)$$

Eq(18) requires that the isotopic content of the solid be continuous as the bulk meets the surface and Eq(19) reflects the fact that the depth of penetration of tracer into the depleted face is very small compared to the specimen thickness.

The solution of Eqs(16) - (19) is:

$$v = \frac{2}{\sqrt{\pi}} \int_{z/2\sqrt{\tau}}^{\infty} u(\eta, \tau - z^2/4\eta^2) e^{-\eta^2} d\eta \quad (20)$$

This is Eq(14) of Ref. 10 with no evaporation and a term $\exp(-\eta^2)$, which had been inadvertently omitted, added. An accurate approximation of the u-function in the integrand is obtained from a two-term Taylor series expansion (10):

$$u(\eta, \tau - z^2/4\eta^2) \cong u(\eta, \tau) - \frac{z^2}{4\eta^2} \frac{\partial u}{\partial \tau} \quad (21)$$

Substituting Eq(21) into Eq(20) and differentiating with respect to Z yields:

$$\left(\frac{\partial v}{\partial z} \right)_{z=0} = - \left(\frac{u}{\sqrt{\pi z}} + \sqrt{\frac{\tau}{\pi}} \frac{\partial u}{\partial \tau} \right) \quad (22)$$

Use of this form in Eq(13) gives:

$$E(\sqrt{\tau} + G) \frac{\partial u}{\partial \tau} = \frac{1}{\eta} \frac{\partial}{\partial \eta} \left(\eta \frac{\partial u}{\partial \eta} \right) - \frac{E}{\sqrt{\tau}} u \quad (23)$$

The initial and boundary conditions are:

$$u(\eta, 0) = 0 \quad (24)$$

$$\left(\frac{\partial u}{\partial \eta}\right)_{\eta=0} = 0 \quad (25)$$

Because of symmetry about the midplane of the duplex specimen, the right hand side of Eq(8) is one half when C_S^+ is replaced by the midplane value $(C_S^+)_m$, or from Eq(7):

$$\left(\frac{\partial u}{\partial \eta}\right)_{\eta=1} = H \left[\frac{1}{2} - u(1, z) \right] \quad (26)$$

where

$$H = ha_{\text{eff}}/D_s \quad (27)$$

is the dimensionless conductance of the periphery of the joint between the two wafers.

As shown in Ref. 10, the solution $u(\eta, \tau)$ obtained (numerically) from Eqs(23) - (26) determines the dimensionless countrate of Eq(1) according to the double integral:

$$R = \frac{4}{\sqrt{\pi}} \int_0^1 (1-z) dz \int_{z/2\sqrt{\tau}}^{\infty} u(\eta, z - z^2/4x^2) e^{-x^2} dx \quad (28)$$

Using Eq(21) permits this integral to be performed and the theoretical

value of R is given by:

$$R = Qu + s \frac{\partial u}{\partial \tau} \quad (29)$$

where, for the small values of τ encountered in the present application:

$$Q = 4\sqrt{\tau} \left(\frac{1}{\sqrt{\pi}} - \frac{\sqrt{\tau}}{2} \right) \quad (30)$$

$$s = -\frac{4}{3\sqrt{\pi}} \tau^{3/2} + \tau^2 \quad (31)$$

The approximate form represented by Eqs(29) - (31) has been compared to numerical integration of Eq(28) and found to be accurate to within a few percent.

DATA ANALYSIS AND RESULTS

The data collected in Table 1 contain information on the three principal physical properties controlling the uranium isotope exchange process, namely the surface diffusion coefficient D_s , the bulk diffusion coefficient D_v and the interfacial conductance h . The surface diffusivity is responsible for the high mobility of the uranium, by which transport over distances characteristic of the specimen diameter in times measured in hours is made possible. Bulk diffusion enters the overall process in two ways. Firstly, it provides a sink term in the uranium surface balance (Eq(6)). Secondly, it controls accumulation of tracer beneath the surface, to which the detection system responds. The surface diffusion process is measurable

only if bulk diffusion of uranium is neither too large nor too small. If bulk diffusion of uranium is rapid, the tracer that enters the surface of the depleted wafer from the enriched one is quickly removed by diffusion into the bulk solid near the wafer-wafer interface and little reaches far onto the face of the depleted wafer. If the bulk diffusion coefficient is small, surface spreading of the tracer across the face of the depleted wafer occurs easily but is not measurable because none is absorbed beneath the surface.

Instead of the physical parameters D_s , D_v and h , fitting of the data in Table 1 to the tracer spreading model was performed using the corresponding dimensionless quantities E , τ , and H . The procedure would have been fairly straightforward were the bulk diffusion coefficient of uranium in UO_2 accurately known, for then the dimensionless time would be a known quantity. Despite many measurements of D_v over the past two decades, Matzke's review (11) demonstrates that a broad band of uncertainty in this property remains. However, it is not totally unknown. Therefore, D_v (or τ) has been permitted to be a semi-free parameter in the data fitting procedure, by which is meant constraining the bulk diffusivity within upper and lower limits estimated from Matzke's compilation (11):

$$0.024 \exp(-93/RT) \leq D_v \leq 0.027 \exp(-87/RT) \quad (32)$$

where D_v is in cm^2/s and the activation energies are in kcal/mole. For each run in Table 1, the above restriction produced a band in which the corresponding dimensionless quantity τ was constrained in the fitting process. The value of the alpha particle range in UO_2 was taken to be $10 \mu\text{m}$ (10).

For each run, the data in Table 1 were fitted according to Eq(4)

and then recast as dimensionless countrates using Eqs(1) and (3). These data were compared to the predictions of the tracer spreading model embodied in Eq(29). The values of E , τ (within the allowable limits) and H needed in the theoretical model were chosen to best fit the data for each run.

The process of extracting values of D_s from the data was aided by the following observations. First, the parameter H is closely related to the slope of the countrate distribution at the wafer edge (See Eq(26) and (29) with the last terms in each neglected). Consequently, good first trials of this parameter could be estimated directly from the data. Second, the data could be satisfactorily fitted to a range of E and τ values with a roughly constant ratio of the two. Thus, despite the lack of a unique set (E , τ , H) which fit the data for each run, a single combination of τ/E and H was obtainable from the data fitting procedure with an accuracy of about 20% on each. As will be seen later, the reproducibility of the experiments was poorer than this, so that the accuracy of the surface diffusion coefficients reported is not limited by the ability to fit the data to the theory. The surface diffusion coefficient was determined from the best-fit value of the ratio of τ to E by use of Eqs(12) and (14):

$$D_s = \frac{(\tau/E)z_F a_{eff}^2}{\sqrt{\pi} t (C_s/C_v)} \quad (33)$$

where the effective wafer radius is defined by Eq(5) and the ratio of superficial and volumetric uranium concentrations for UO_2 (i.e., C_s/C_v)

is 2.7×10^{-8} cm.

Figure 2 shows the steps in the fitting process for the temperature variation runs in Table 1. In each graph, the count rate data and the polynomial fit by Eq(4) are shown on the left. In some cases both two- and three-parameter fits could be obtained. However, these fits were indistinguishable from each other on the scale of the drawing and are shown as single curves. The points on the right hand portions of the drawings correspond to the radial distributions of the dimensionless count rate obtained from Eqs(1) and (3). While these points do not strictly speaking represent discrete data, they have been plotted as such to facilitate comparison with the theoretical results. In the case that the original data were fitted to both two- and three-parameter polynomials, slight differences in the goodness of the fits which were not visible on the left hand plots are magnified and produced distinct sets of points on the right hand plots. The curves on the right hand plots are the results of the model calculations for the two or three combinations of parameters which best fit the data.

Run numbers 5 and 6 are plotted on the same graph in Fig. 2 because they represent replicate experiments. Except for these runs and the highest temperature experiment (run 8), very close model fits to the data were obtained. The raw data for run 8 do not appear different in general shape from those for the experiments at lower temperatures, but the dimensionless count rate distribution derived from these data is concave downward rather than concave upward. The former shape cannot be properly fitted by the theory.

Table 2 summarizes the parameters of the best-fitting theoretical curves shown on the right hand sides of the graphs in Fig. 2. Despite

the range of E and τ values which can fit the same set of data, the τ/E ratios for a particular experiment are generally much less variable. The surface diffusion coefficients calculated from Eq(33) are listed in the last column of Table 2 and are plotted in Fig. 3. Also shown on this graph is the datum at 1915°C obtained by Marlowe and Kaznoff (6) after reinterpretation in Ref. 10 by the same type of theoretical model as was applied to the present data. The good agreement between the results of the two tracer experiments demonstrates that the theoretical model used for analysis of the data can accommodate quite different geometries of the diffusion couple. The good accord also shows that neither evaporation of the specimens nor isotope movement by vapor transport affected the present tests or those of Marlowe and Kaznoff. Not only did the close-fitting rhenium foils (Fig. 1) prevent transport in the gas phase, but they did not introduce spurious effects such as impeding surface diffusion by physically contacting the UO_2 surfaces or providing a parallel surface diffusion pathway.

The diffusion coefficient can be expressed in Arrhenius form;

$$D_s = D_{s0} \exp(-E_s/RT) \quad (34)$$

The line through the data in Fig. 3 corresponds to $D_{s0} = 5 \times 10^6 \text{ cm}^2/\text{s}$ and $E_s = 72 \text{ kcal/mole}$. Although the deviations of the data points from the line are generally within $\pm 50\%$, the errors in the coefficients in Eq(34) are larger. The accuracy of E_s is estimated to be $\sim \pm 15 \text{ kcal/mole}$ and D_{s0} is not known to better than one or two orders of magnitude about the mean value. Nevertheless, both the preexponential factor and the activation energy are significantly smaller than previous measurements of surface diffusion on UO_2 (4,5).

The value of τ listed in Table 2 which provided the best fitting model curves correspond to bulk diffusion coefficients which are plotted in Fig. 4 as bars for each run along with the bounding lines given by Eq(32). Adequate data interpretation was achieved with values of D_v

within the range of previous measurements from the literature (11). The bulk diffusivities of the urania in the duplex specimen used in the present work are on the low side of the band representing the results of experiments designed solely to measure this property. However, the bars in Fig. 4 should not be construed as measurements of D_v .

Figures 5 - 8 and Table 3 show the data and the derived surface diffusion coefficients for the measurements in a variety of atmospheres at a fixed temperature. As in the previous tests in wet hydrogen at varying temperature, the theory was readily fitted to the data. There does not, however, appear to be a clear effect of the ambient gas (or lack of it) on the surface diffusion coefficient. Except for the result in argon, the D_s values in Table 3 are lower than the range of values of D_s in wet hydrogen at the same temperature. The limited extent of tracer movement in helium and vacuum environments is unexpected. Note that these gases contained no reducing agent nor were they highly dried prior to introduction into the furnace.

Examination of the values of the interfacial resistance parameter (H) given in Tables 2 and 3 shows no particular variation with either temperature or gaseous environment. Values between 0.02 and 0.15 appear in both Tables. The extent to which the resistance of the joint impedes surface movement of uranium between the enriched and depleted wafers comprising the diffusion couple can be assessed by calculating the dimensionless countrate expected at the specimen periphery had there been a perfect joint. If H were very large, Eq(26) shows that $u(1, \tau) = \frac{1}{2}$ and Eq(29) reduces to $R(\eta=1) = Q/2$, where, for small τ , $Q = 4(\tau/\pi)^{1/2}$. If the interface had offered no transport resistance, at the experimental τ values ranging from 0.02 to 0.04 (Table 2), values of R at $\eta = 1$ between 0.2 and 0.4 should have been observed. However, examination of

of the right hand plots in Fig.2 shows that the actual dimensionless count-rates at a fractional radius of one are less than 5% of these values. The interface is thus a larger impediment to surface spreading of uranium isotopes than is surface diffusion.

DISCUSSION

The very large preexponential factor for surface diffusion on UO_2 is characteristic of many ceramic oxides(7). In the framework of the conventional site-to-site hopping mechanism of atom migration universally applicable to volume diffusion in solids, the large preexponential factor implies an enormous jump distance on the surface. Similar observations have been reported for surface diffusion on some metals, for which Bonzel(17) developed a theory of surface diffusion out which naturally arises very large preexponential factors.

Bonzel's model is based upon the assumption that only surface atoms (or polyatomic units built up from the atoms or ions of the crystal) which are in an adsorbed state (adatoms) are responsible for surface mobility. The vast majority of the $\sim 10^{15}$ surface atoms per square centimeter form part of the terrace-ledge-kink surface structure. An equilibrium fraction of surface atoms in the adatom state (f_a) is maintained by the ledges acting as source and sink:

$$f_a = \exp(\Delta S_a/R) \exp(-\Delta H_a/RT) \quad (35)$$

where R is the gas constant and ΔS_a and ΔH_a are the entropy and enthalpy of formation of the adatoms from the atoms in the surface. Surface-adsorbed single atoms are treated as three-dimensional oscillators with two degrees of vibrational motion parallel to the surface and a third normal to it. An adsorbed molecule such as a UO_2 possesses these three center-of-mass vibrational modes but in addition exhibits internal vi-

brational modes.

The surface diffusion coefficient is given by:

$$D_s = f_a D^* \quad (36)$$

where D^* is the intrinsic diffusion coefficient of the adatom. This formulation is analogous to the "equilibrium trapping" model frequently applied to fission gas diffusion in UO_2 (18). Bonzel shows how to calculate D^* for the case of localized motion (hopping one lattice position at a time) and for the case of nonlocalized migration, in which long distances are traversed between leaving and returning to the adatom state. Only the latter mechanism produces large preexponential factors characteristic of surface migration on UO_2 .

Bonzel's model starts from the equation for the intrinsic diffusion coefficient of the adatom in nonlocalized motion obtained from random walk theory:

$$D^* = \alpha \ell^2 \Gamma \quad (37)$$

where α is a geometrical constant (set equal to unity), and ℓ and Γ are the jump distance and the jump frequency, respectively. These two properties of the adatom are determined with the aid of absolute rate theory, according to which motion occurs by population of an activated state from the adatom state. The nonlocalized activated state is a two-dimensional zone with an area of approximately one lattice constant squared. A molecule in this state has an energy ΔH^* above that of the equilibrium adatom state (Fig. 9). The average two-dimensional thermal velocity of the molecules in the activated

state is:

$$v = 2 \sqrt{\frac{kT}{\pi m}} \quad (38)$$

where k is Boltzmann's constant and $m = 4.5 \times 10^{-22}$ g is the mass of the UO_2 molecule. The intrinsic diffusion coefficient obtained by Bonzel is:

$$D^* = \frac{\alpha v^2}{v_{\perp}} \left(\frac{z^*}{z_a} \right) \exp\left(-\frac{\Delta H^*}{RT}\right) \quad (39)$$

where v is the vibration frequency of the equilibrium adatom perpendicular to the surface and z_a is its partition function:

$$z_a = \left(\frac{kT}{h\nu_{\perp}} \right) \left(\frac{kT}{h\nu_{11}} \right)^2 z_{\text{int}}^{\text{vib}} \quad (40)$$

where h is Planck's constant, ν_{11} is the frequency of adatom vibration parallel to the surface and $z_{\text{int}}^{\text{vib}}$ is the partition function representing the three internal vibrational modes of the linear UO_2 molecule stretching and bending modes, (see Ref. 19). The form of the center-of-mass vibrational partition functions in Eq(40) assumes that $kT \gg h\nu$, which appears to be a satisfactory simplification. The degrees of freedom of the molecule in the nonlocalized activated state include vibration normal to the surface, internal vibrational modes, two translational modes, and rotational modes. The first two of these are present in the adsorbed state, but the two parallel vibrational modes of the equilibrium adsorbed species have been replaced by two translational modes and two rotational modes in the activated state.

The partition function of the activated state is:

$$z^* = \left(\frac{kT}{v_{\perp}^*} \right) z_{\text{int}}^{\text{vib}} \left(\frac{2\pi mkT_A}{h^2} \right) \left(\frac{T}{2\theta_{\text{rot}}} \right) \quad (41)$$

where $A = 1.5 \times 10^{-15} \text{ cm}^2$ is the area per surface uranium atom in the close-packed planes of the UO_2 structure. The quantity θ_{rot} is the temperature characterizing the two degrees of freedom for unhindered rotation of the UO_2 molecule in the activated state on the surface. This quantity can be calculated from a standard statistical-mechanical formula for a linear molecule provided that the moment of inertia is known. The latter depends on the masses of the particles at each end of the molecule (oxygen atoms) and on the uranium-oxygen bond distance (1.79 \AA , Ref. 19). The rotational temperature of the UO_2 molecule is calculated to be 0.24 K .

Assuming $v_{\perp}^* = v_{\perp}$ and $z_{\text{int}}^{\text{vib}}$ to be the same in the equilibrium adatom and the activated states, the partition function ratio in Eq(39) becomes:

$$\frac{z^*}{z_a} = \frac{\left(\frac{2\pi mkT}{h^2} A \right) \left(\frac{T}{2\theta_{\text{rot}}} \right)}{\left(\frac{kT}{h\nu_{11}} \right)^2} \quad (42)$$

Taking T to be the average temperature of the tracer spreading experiments (2200 K) and assuming $\nu_{11} = 10^{13} \text{ s}^{-1}$, the partition functions in the above equation are $30,000$ for translation, 4600 for rotation and $(4.6)^2$ for vibration. The ratio z^*/z_a is 6.5×10^6 . Taking $\alpha = 1$, calculating $v = 2.9 \times 10^4 \text{ cm/s}$ from Eq (38) and assuming $v_{\perp} = 10^{13} \text{ s}^{-1}$, the pre-

exponential factor of D^* in Eq(39) is $D_0^* = 3.6 \times 10^9 \text{ cm}^2/\text{s}$.

According to Eqs(35) and (36), the preexponential factor of D_s is equal to $D_0^* \exp(\Delta S_a/R)$. In the case of a metal lattice supporting a population of single adsorbed atoms, Bonzel takes $\Delta S_a = 1.5R$, in which is implicit the reasonable expectation that little change in the vibrational entropy occurs when an atom is moved from a kink site to an adsorbed site. For uranium dioxide, on the other hand, the moving unit is assumed to be the neutral UO_2 molecule, and the entropy change associated with assembling this surface-adsorbed species from the constituent ions in the surface structure may be very much different from that for producing an adatom on a metal surface.

The entropy change ΔS_a can be computed from the thermodynamic cycle shown in Fig. 9, which gives:

$$\Delta S_a = \Delta S_v - (S_g - S_a) \quad (43)$$

where $\Delta S_v = 39.3 \text{ eu}$ is the entropy of vaporization of UO_2 and S_g is the absolute entropy of the UO_2 molecule in its gaseous standard state, which consists of contributions due to translation, rotation and internal, rotation and internal vibrations:

$$S_g = S_{\text{tr}} + S_{\text{rot}} + S_{\text{vib}}^{\text{int}} \quad (44)$$

The entropy of the adsorbed UO_2 molecule is:

$$S = S_{\text{vib}}^{\text{COM}} + S_{\text{vib}}^{\text{int}} \quad (45)$$

The last terms in Eqs(44) and (45) represent the entropy due to inter-

nal vibrations of the UO_2 molecule, which is assumed to be the same in the adsorbed and gaseous states. The entropy of formation of the surface-adsorbed UO_2 molecules is thus:

$$\Delta S_a = \Delta S_v - S_{tr} - S_{rot} + S_{vib}^{COM} \quad (46)$$

The translational entropy of the ideal gas can be calculated from statistical mechanical formulas. At the standard conditions of 1 atm pressure and 2200 K, $S_{tr} = 52.7$ eu. The rotational and vibrational entropy contributions are calculated from the formula:

$$S = R \left(\ln z + \frac{d \ln z}{d \ln T} \right) \quad (47)$$

where z is the appropriate partition function. Using the last term in Eq(41) for z_{rot} , Eq(47) yields $S_{rot} = 18.7$ eu at 2200 K. Applying the same formula to the center-of-mass vibrational partition functions in Eq(40) (taking $\nu_1 = \nu_{11} = 10^{13} \text{ s}^{-1}$ and $T = 2200$ K) yields $S_{vib}^{COM} = 15.0$ eu.

Substituting the numerical values of the component entropies determined above into Eq(46) gives $\Delta S_a = -17.1$ eu. The large negative entropy of formation of the UO_2 is a reflection of the more organized state of the neutral UO_2 molecule compared to U^{4+} and O^{2-} ions in the crystal lattice at the surface. For comparison, the same method can be used to compute the entropy of formation of copper adatoms on $\text{Cu}(110)$. In this case, the component entropies (at 1200K) are: $\Delta S_v = 30.3$ eu; $S_{tr} = 45.5$ eu; $S_{rot} = 0$; $S_{vib}^{COM} = 17.7$ eu (using the adatom vibration frequencies recommended by Bonzel(17)). Inserting these values into Eq(46) yields $\Delta S_a = 2.5$ eu, which is in good agreement with the value of 3.0 eu used by Bonzel.

The theoretical preexponential factor in Eq(34) is:

$$D_{sO} = D_0^* \exp(\Delta S_a/R) = 3.6 \times 10^9 e^{-17.1/R} = 6.6 \times 10^5 \text{ cm}^2/\text{s}$$

If the calculation is repeated with a COM vibration frequency of $5 \times 10^{12} \text{ s}^{-1}$, the resulting calculated value of D_{sO} is $7.6 \times 10^5 \text{ cm}^2/\text{s}$.

Comparing these theoretical values with the observed Arrhenius form of D_s given by Eq(34), the preexponential factor is seen to be underpredicted by a factor of ~ 7 . This discrepancy corresponds to an error of ~ 4 eu in ΔS_a or in the corresponding entropy terms in D_0^* . Noting that these entropies result from adding and subtracting a number of fairly large component entropies, an error of 4 eu is not unreasonable. In addition the accuracy of the experiment preexponential factor is larger than the discrepancy with theory. In sum, it can be concluded that Bonzel's model of nonlocalized surface diffusion applies quantitatively to UO_2 if the migrating species used in the computations is the neutral UO_2 molecule.

According to the diffusion model, the observed activation energy of surface diffusion is the sum of the enthalpy of formation of the adatom and the activation enthalpy of the nonlocalized state:

$$E_s = \Delta H_a + \Delta H^* \quad (49)$$

Not enough is known about the interatomic forces on the UO_2 surface to permit calculation of either of the two terms on the right hand side OF Eq(49). The experimental results show only that their sum is ~ 72 kcal/mole.

The model calculations described above were based upon the assumption that the adatom is the UO_2 molecule. A similar calculation can be performed with the U^{+4} ion as the migrating species. In this case, the entropy of formation of the equilibrium adatom is approximated by

the 3 eu which characterizes the copper adatom. However, the partition function for the activated state contains no rotational component, so the second term in the numerator of Eq(42) is removed in computing z^*/z_a . The resulting theoretical value of D_{SO} is $<10^3 \text{ cm}^2/\text{s}$, far smaller than the experimental result. It appears that the rotational stabilization achievable only by a polyatomic entity such as the UO_2 molecule is necessary for the high surface mobility on this oxide.

A consequence of Bonzel's model which bears examination is the "jump distance" in Eq(37). For surface diffusion by the nonlocalized mode, this quantity is more precisely termed the mean free path in the two-dimensional gas between activation and deactivation. The theory is not specific on the cause of deactivation of the moving species. Bonzel suggests collision with another moving molecule, a two-dimensional analog of the principal event in a common three-dimensional ideal gas. Or, the moving molecule may encounter a localized adatom. However, Bonzel's model does not allow for the effect of morphological features of the surface on the mean free path of the migrating species. Such features include ledges, emerging dislocations, impurity atoms on the surface, and grain boundaries. Were any of these defects to serve as collision partners for the moving species, the mean free path of the latter would depend on a measure of the density of the obstacles, as neutron diffusion in a moderator is dependent on the density of moderator atoms. Bonzel's theory does not permit this type of deactivation, but instead determines the mean free path solely from the properties of the surface molecule in the adatom and activated states. The mean free path can be obtained by equating the right hand sides of Eqs(37) and (39) and using $\Gamma = v_{\perp} \exp(-\Delta H^*/RT)$, leading to:

$$l = \frac{v}{v_{\perp}} \frac{z^*}{z_a} \quad (49)$$

All of the quantities on the right hand side of this equation have been calculated previously. Their use gives mean free path between 100 and 200 μm , depending on the value of v employed. Application of Bonzel's to UO_2 implies that an activated UO_2 molecule can travel as an ideal gas particle for distances which traverse 10 to 20 grain boundaries, not to mention a much larger number of small structural defects which undoubtedly are present on the grain faces. The theory thus suggest a remarkably deactivation-resistant surface species on UO_2 . Since Bonzel's theory is structure-insensitive, surface diffusion on single crystals of uranium dioxide should be the same as on polycrystals. The feature of the theory remains to be tested.

Another extrinsic mechanism of deactivation of moving surface species is collision with gas atoms impinging on the surface. The series of experiments in which the ambient gas was varied was intended to examine this possibility. It is reasonable to assume that the surface diffusivity decreases with increasing frequency of collision of gas atoms with the surface in a manner similar to the inverse dependence of gas phase diffusion on total pressure. Accordingly, D_s should be largest in a vacuum, change in a regular fashion as the atomic weight of the gas is varied at constant pressure, and decrease with increasing pressure of a single gas. The present experiments bore out none of these expectations, so it is useful to query the theory to ascertain whether a change of sufficient magnitude to stand out from experimental uncertainties should have been expected in the conditions of the gas-variation tests.

In a vacuum, the moving species has a natural mean free path on the surface (Eq(49)) which is independent of the environment. To determine how this flight path is shortened by the presence of a gas above the solid, the probability of premature deactivation by collision with impinging gas atoms is calculated. This probability is the prod-

duct of two others. The first is the probability that a moving surface molecule is struck by an impinging gas atom and the second is the probability that the collision removes sufficient energy from the former to cause it to return to the bound atom state.

During its flight across the surface, a moving atom presents a rectangular area of length equal to its natural mean free path ℓ and width equal to the collision diameter with the gas atom, σ . Assuming hard sphere collisions, the collision diameter is the sum of the molecular diameter of the UO_2 molecule (d_U) and the atomic diameter of the gas atom (d_g):

$$\sigma = d_U + d_g \quad (50)$$

If a gas atom strikes the area $\sigma\ell$ while the surface molecule is moving across its track, a collision is possible.

The impingement rate of the gas on the surface for 1 atm pressure and 2200 K is:

$$Q = \frac{P}{\sqrt{2\pi m_g kT}} = \frac{5.7 \times 10^{23}}{\sqrt{M_g}} \quad \text{atoms/cm}^2 \text{ -s} \quad (51)$$

where M_g is the atomic weight of the gas. The lifetime of the moving molecule on the surface is ℓ/v , where v is its thermal velocity, so that the total number of gas atoms which strike the path of the moving molecule during its flight along its natural path length is $Q(\sigma\ell)$ (ℓ/v). The probability that any one of these impinging atoms collides with the moving surface molecule is the ratio of the collision diameter to the path length, or to σ/ℓ . Multiplying these two probabilities, the probability that a moving surface molecule is struck by an impinging

gas atom before it naturally deactivates is:

$$P_{\text{coll}} = \frac{Q\ell\sigma^2}{v} \quad (52)$$

Taking $M_g = 132$ (for xenon), $\sigma = 4 \text{ \AA}$, $\ell = 150 \text{ \mu m}$, and $v = 2.9 \times 10^4 \text{ cm/s}$, Eq(52) gives a $p_{\text{coll}} \sim 40$, implying a very high likelihood of a collision. Because of the atomic weight factor in Eq(51), the collision probability is even higher for gases lighter than xenon.

However, not every collision need result in deactivation. Energy transfer in the collision is more efficient for the heavy species (which have masses closer to that of the UO_2 molecule) than the lighter ones, as determined by the energy transfer factor $4M_g M_U / (M_g + M_U)^2$, where M_U is the molecular weight of UO_2 . Lacking knowledge of the energy transfer mechanism in such collisions and the translational energy that must be removed from the moving surface molecule to cause deactivation, quantitative assessment of the probability of deactivation in a collision is not possible. However, it is quite likely that the lighter gases are less efficient in this respect than the heavier ones. In addition, the probability of removing an appreciable fraction of the activation enthalpy ΔH^* of the moving UO_2 molecule by collision with a gas atom is undoubtedly considerably less than unity, so the product of this factor and p_{coll} of Eq(52) may also be less than one. If so, the theory would be consistent with the failure to observe a significant effect of the gaseous environment on surface diffusion. However, if the gas pressure were very high, as it is in fission gas bubbles, it is possible that the correspondingly larger collision probabilities could cause a decrease in surface mobility, as postulated in Refs. 12-14.

CONCLUSIONS

The surface diffusion coefficient on polycrystalline UO_2 has been determined by measurement of the spreading of tracer uranium on the surface of a duplex specimen composed of enriched and depleted UO_2 wafers. Surface diffusivities were determined from the data by means of a phenomenological model which included simultaneous bulk diffusion and an interface resistance between the two wafers. The surface diffusion coefficients over the temperature interval from 1760 to 2100°C range from ~ 0.1 to ~ 2 cm^2/s . The quantity needed in analyses of mass transport along the surface is the product of D_s and the surface layer thickness δ , which in the present model is equal to the ratio of the areal density of uranium atoms on the surface to the bulk uranium atom density in the solid. This ratio is $\sim 3 \text{ \AA}$. Consequently, the product δD_s varies from 3×10^{-9} to 6×10^{-8} cm^3/s over the temperature range investigated.

Bonzel's theory of nonlocalized surface migration was applied to the measurements and was found to be capable of explaining the large preexponential factor of D_s provided that the migrating species is the UO_2 molecule capable of free rotation. However, a consequence of this requirement is a long mean free path of the migrating molecule on the surface, which covers distances equivalent to many grains between activation to the nonlocalized mobile state and deactivation back to the bound adatom state. This very large predicted mean free path is directly related to the assumption of unhindered rotation of the activated UO_2 molecule on the surface. If one degree of rotational freedom is removed from the partition function z^* , a physically acceptable (but still quite large) mean free path results. However,

removal of one degree of rotational freedom results in a substantial decrease in the calculated preexponential factor, and agreement of experiment with theory is lost. In order to reduce the mean free path by invoking hindered rotation yet maintain the necessary large preexponential factor, a smaller entropy of formation of the bound adatom state (ΔS_a) than the value of -17 eu estimated from available information on UO_2 vaporization would be needed.

The effect of the nature of the ambient gas on D_s , if such an effect was present, was less than the precision of the measurements. The absence of this affect could be rationalized by the theory, however.

ACKNOWLEDGEMENT

This work was supported by the Direct, Office of Energy Research, Office of Basic Energy Sciences, Materials Sciences Division of the U.S. Department of Energy under contract #DE-AC03-76SF0098.

REFERENCES

1. G.L. Reynolds, J. Nucl. Mater. 24 (1967) 69.
2. I. Amoto, R.L. Columbo and G.C. Grappiolo, Solid State. Comm. 4 (1968) 237.
3. J. Henney and J.W.S. Jones, J. Mater. Sci. 3 (1968) 158.
4. P.S. Maiya, J. Nucl. Mater. 40 (1971) 57.
5. E.N. Hodkin and M.B. Nicholas, J. Nucl. Mater. 47 (1973) 23.
6. M.O. Marlowe and A.I. Kaznoff, J. Nucl. Mater. 25 (1968) 328.
7. W.M. Robertson, J. Nucl. Mater. 30 (1969) 36.
8. P.G. Shewmon, J. App. Phys. 34 (1963) 755.
9. R.M. Berman, Trans. Am. Nucl. Soc. 12 (1969) 78.
10. D.R. Olander, J. Nucl. Mater. 96 (1981) 243.
11. Hj. Matzke, J. Nucl. Mater. 114 (1983) 121.
12. B.J. Buescher and R.O. Meyer, J. Nucl. Mater. 48 (1973) 143.
13. E. Ya. Mikhlin, J. Nucl. Mater. 87 (1979) 405.
14. W. Nixon and D.A. MacInnes, J. Nucl. Mater. 101 (1981) 182.
15. H. Furaya and M. Koizumi, in: Thermodynamics of Nuclear Materials (IAEA, Vienna, 1974) p. 447.
16. Hj. Matzke and R.A. Lambert, J. Nucl. Mater. 64 (1977) 211.
17. H.P. Bonzel, Surf. Sci., 21 (1970) 45.
18. D.R. Olander, "Fundamental Aspects of Nuclear Reactor Fuel Elements", Tech. Info. Div., U.S. Dept. of Energy (1976) 307.
19. D.W. Green, "Calculation of the Thermodynamic Properties of Fuel-Vapor Species from Spectroscopic Data", ANL-CEN-RSD-80-2 (1980).

TABLE 1

DATA SUMMARY

RUN NO.	6	5	4	3	2	1	7	8	9	10	11	12	13
TEMP. °C	1760	1760	1814	1818	1914	1919	2005	2110	1813	1817	1811	1816	1814
TIME, MIN.	120	120	90	120	60	60	20	15	60	60	60	60	60
ATMOSPHERE	Sat'd H ₂	Sat'd H ₂	Sat'd H ₂	Sat'd H ₂	Sat'd H ₂	Sat'd Ar-4%H ₂	Sat'd H ₂	Sat'd H ₂	Xe	Kr	Ar	He	Vac.
RADIUS OF APERTURE, cm	COUNTS IN 8 MIN-UNMASKED ZONE												
0.146	1008	905	1040	1613	1151	1695	1074	1474	886	957	999	926	913
0.201	1824	1804	1945	3072	1940	3358	1929	2978	1753	1784	1987	1686	1739
0.256	2911	2907	3046	4918	3390	5425	3334	4937	2801	3046	3237	2763	2869
0.290	3730	3865	3973	6710	4325	7135	4338	6788	3864	3962	4181	3696	3764
0.405	7560	7483	6594	13271	8367	14328	8922	14600	7475	7813	8256	7177	7386
0.497	11278	11270	11603	21095	12557	22195	14112	22871	11446	12069	12794	10910	11125
0.564	14453	14744	14903	28490	16791	29406	19105	30365	15419	15781	16848	14551	14324
0.627	18088	18525	18325	36807	22521	37605	25033	39111	20289	20729	21437	19125	18392
0.704	23237	23759	23642	48906	32675	50666	-	-	-	-	-	-	-

Preanneal 8 minute counts per cm² (all runs):

Enriched face: 2,360,000 ± 5400

Depleted face: 12,900 ± 80

Sample Geometry:

Radius: 0.73 cm (Run. Nos. 1-6); 0.69 cm (Run Nos. 7 - 13)

Thickness of each disk: 0.1 cm

TABLE 2

RESULTS

FOR THE TEMPERATURE DEPENDENCE OF THE SURFACE DIFFUSIVITY

<u>RUN NO.</u>	<u>TEMP., °C</u>	<u>KEY*</u>	<u>E</u>	<u>τ</u>	<u>H</u>	<u>τ/E</u>	<u>$D_s, \text{cm}^2/\text{s}$</u>
6,5	1760	1	.4	.018	.02	.045	
		2	.45	.021	.02	.047	
		3	.5	.024	.02	.048	
						AVG=.047	
4	1814	1	.4	.018	.02	.045	
		2	.5	.023	.02	.046	
		3	.6	.030	.02	.050	
						AVG=.047	
3	1818	1	.5	.05	.08	.10	
		2	.6	.06	.08	.10	
		3	.7	.075	.08	.11	
						AVG=.110	
2	1914	1	2.5	.08	.12	.032	
		2	2.5	.06	.15	.024	
		3	3.0	.10	.12	.033	
						AVG=.030	
1	1919	1	.6	.075	.08	.13	
		2	.8	.11	.07	.14	
		3	1.0	.22	.05	.22	
						AVG=.147	
7	2005	1	.7	.025	.10	.036	
		2	1.0	.034	.10	.034	
						AVG=.035	
8	2110	1	.5	.06	.07	.14	
		2	.5	.09	.05	.18	
		3	.7	.135	.05	.19	
						AVG=.17	

* The numbers correspond to the numbered curves in Fig. 2.

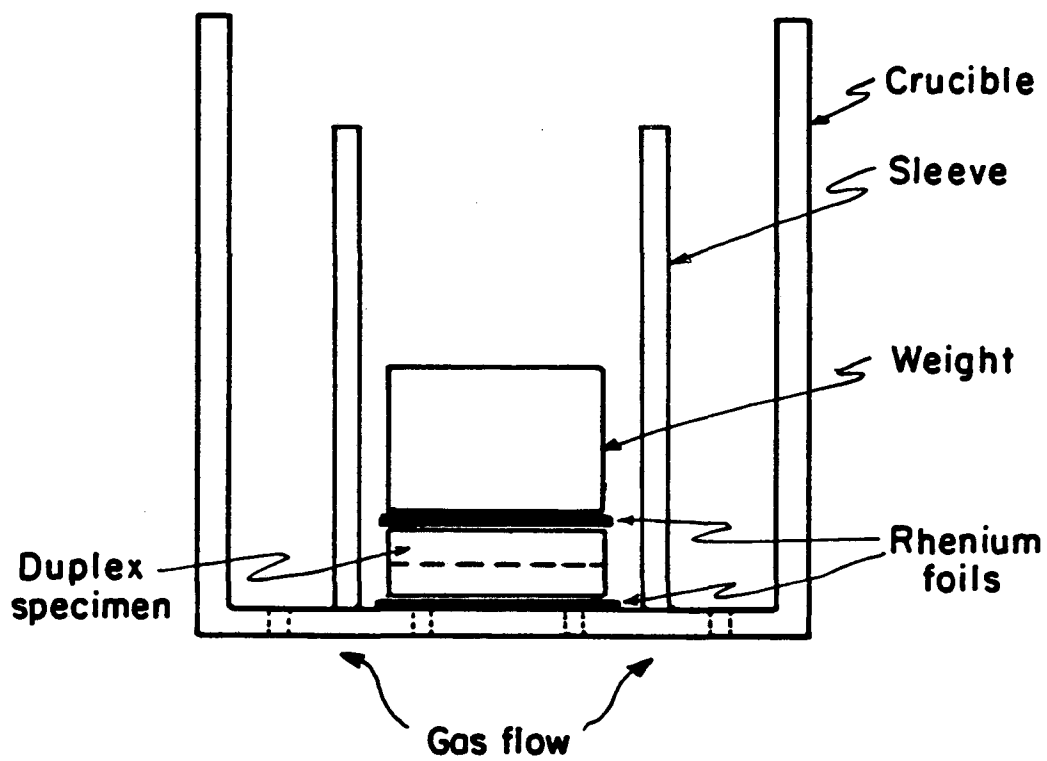
TABLE 3
EFFECT OF GASEOUS ENVIRONMENT

AT T= 1814°C
t= 1 h

<u>RUN NO.</u>	<u>GAS</u>	<u>KEY*</u>	<u>E</u>	<u>τ</u>	<u>H</u>	<u>τ/E</u>	<u>$D_s, \text{cm}^2/\text{s}$</u>
9	Xe	1	1.25	.018	.12	.014	
		2	1.50	.030	.08	.020	
		3	1.50	.024	.12	.016	
		4	1.75	.040	.08	<u>.023</u>	
						Avg = .018 ± .004	.063
10	Kr	1	0.75	.017	.08	.023	
		2	1.00	.023	.07	.023	
		3	1.25	.038	.06	<u>.038</u>	
						Avg = .025 ± .003	.089
11	Ar	1	0.60	.03	.06	.050	
		2	0.75	.04	.04	<u>.053</u>	
						Avg = .052 ± .001	.180
12	He	1	2.0	.025	.10	.013	
		2	2.5	.030	.08	.012	
		3	3.0	.060	.07	<u>.020</u>	
						Avg = .015 ± .004	.052
13	Vacuum	1	0.5	.010	.04	.020	
		2	0.5	.014	.03	.028	
		3	0.6	.017	.03	<u>.028</u>	
						Avg = .025 ± .004	.087

* The numbers corresponds to numbered curves in Figs. 5 - 8

1. Duplex-wafer diffusion couple with rig for annealing in a furnace. The crucible, sleeve and weight are fabricated of molybdenum.
2. Fitting of tracer spreading data for the experiments in flowing wet hydrogen at various temperatures. The curves through the points (o) in the left hand panels represent 2-or 3-parameter polynomial fits. The points in the right hand panels were obtained from the polynomial fits on the left: ▲ 2-parameter; ● 3-parameter. The curves on the right are theoretical; the numbers identifying each give the parameters used in the computation by referring to Table 2.
3. Tracer surface diffusion coefficients on UO_2 in wet hydrogen atmospheres.
4. Volume diffusion coefficients used in determining surface diffusivity. The band corresponds to Eq(32).
5. Fitting of tracer spreading data at $1813^\circ C$ in xenon gas at 1 atm. Two-parameter fit to data.
6. Fitting of tracer spreading data at $1817^\circ C$ in krypton gas at 1 atm. Two-parameter fit to the data.
7. Fitting of tracer spreading data at $1811^\circ C$ in argon gas at 1 atm. Two-parameter (●) and three-parameter (▲) fits to the data.
8. Fitting of tracer spreading data at $1816^\circ C$ in helium at atm (top) and at $1814^\circ C$ in vacuum (bottom). Two-parameter fits to the data.
9. Thermodynamic cycle for determining the adatom entropy of formation.



XBL 834-5489

Figure 1.

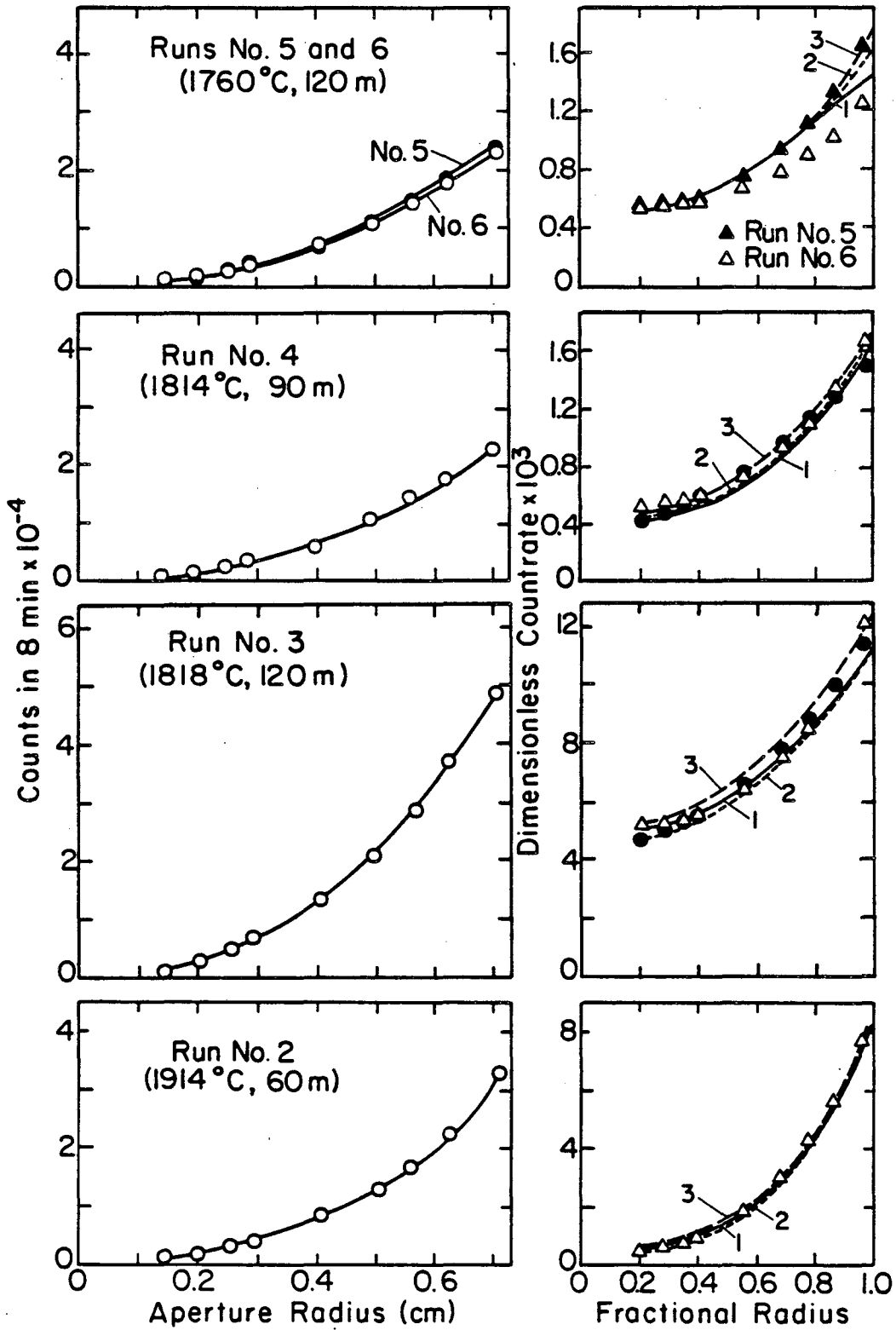
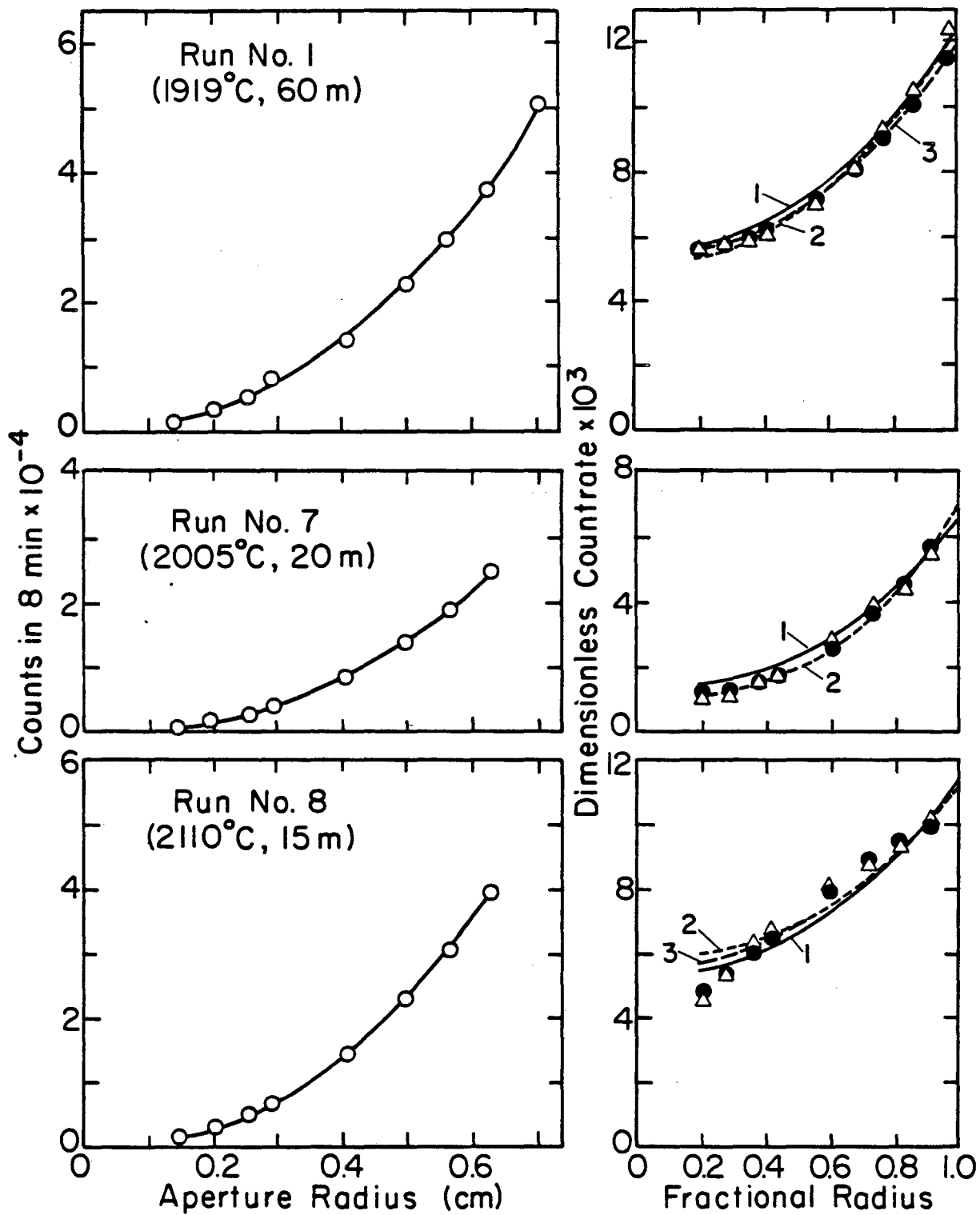


Figure 2.



XBL 834-5496

Figure 2 (continued)

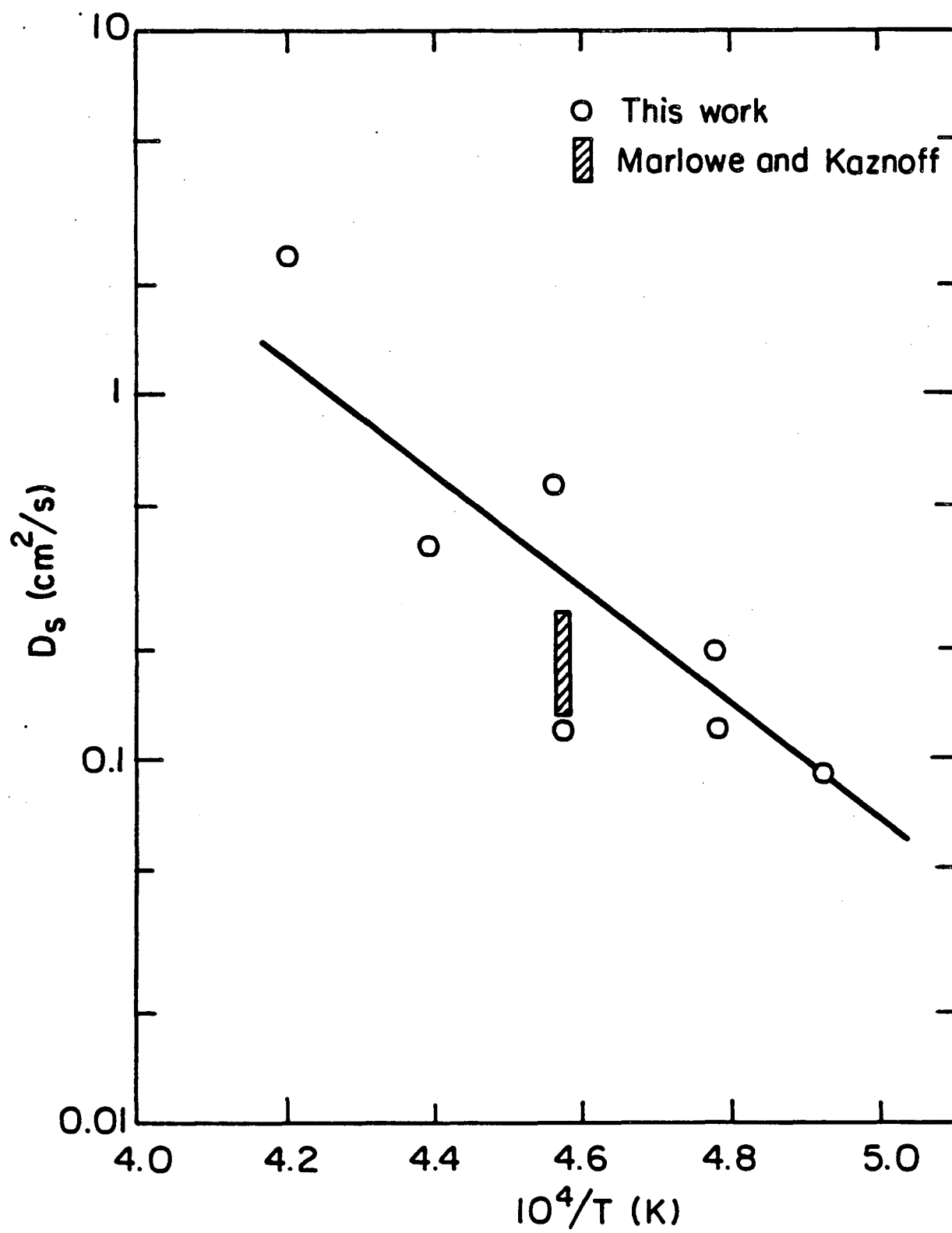
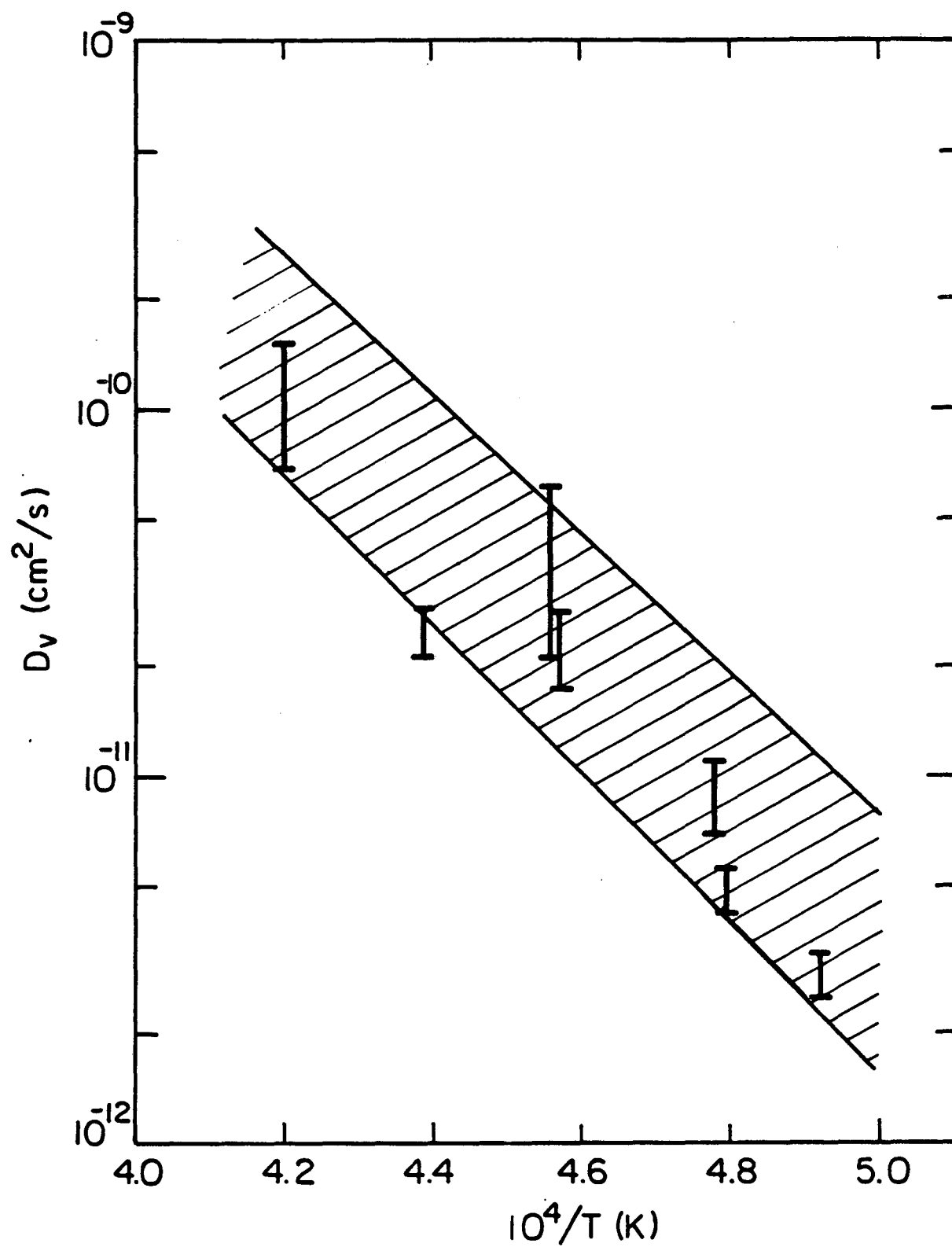
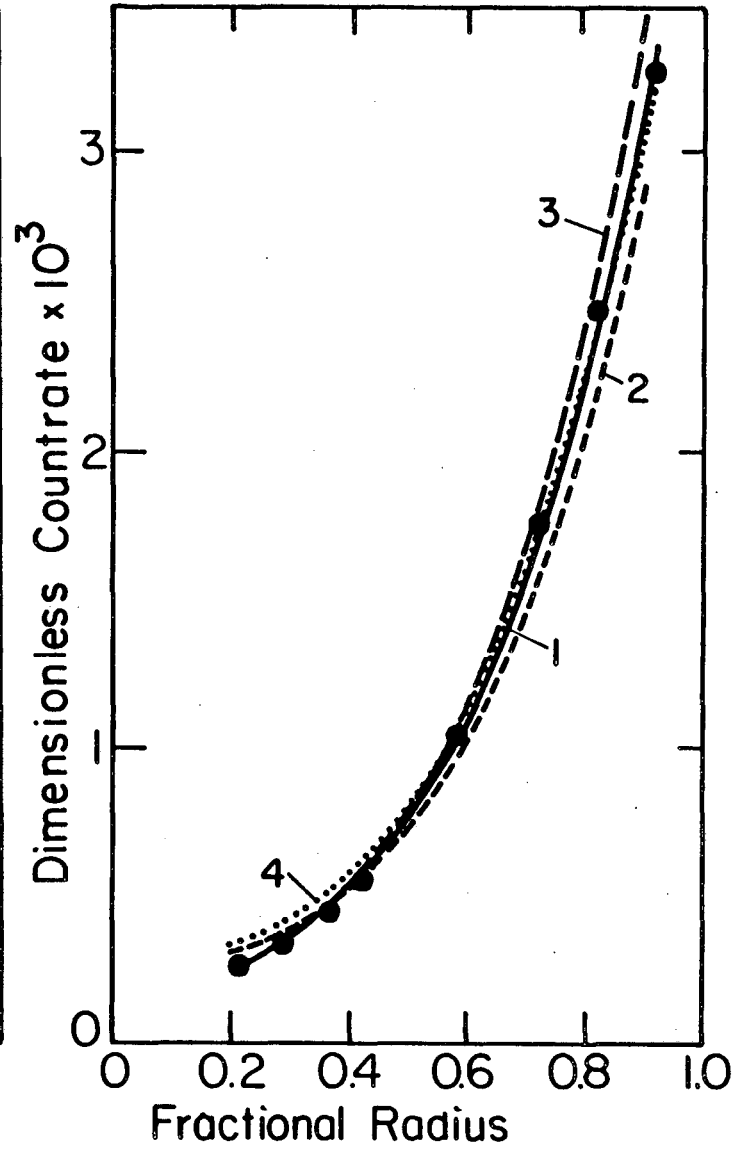
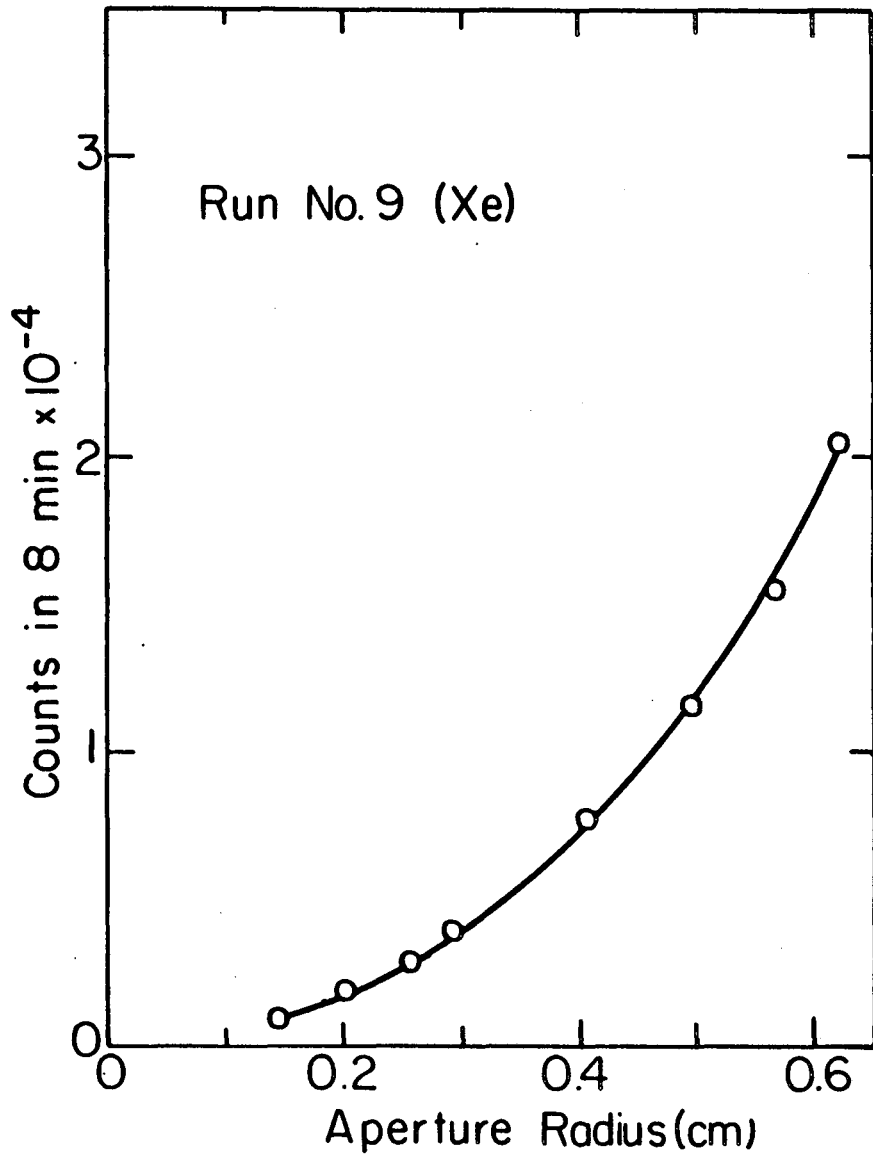


Figure 3.



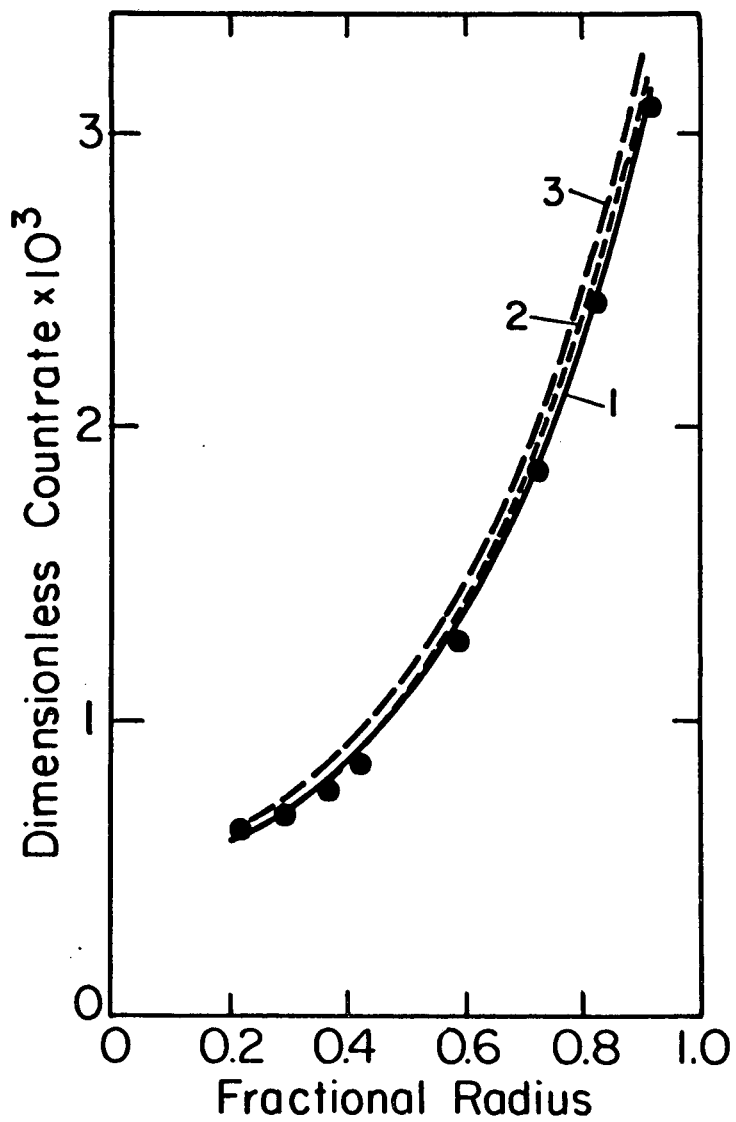
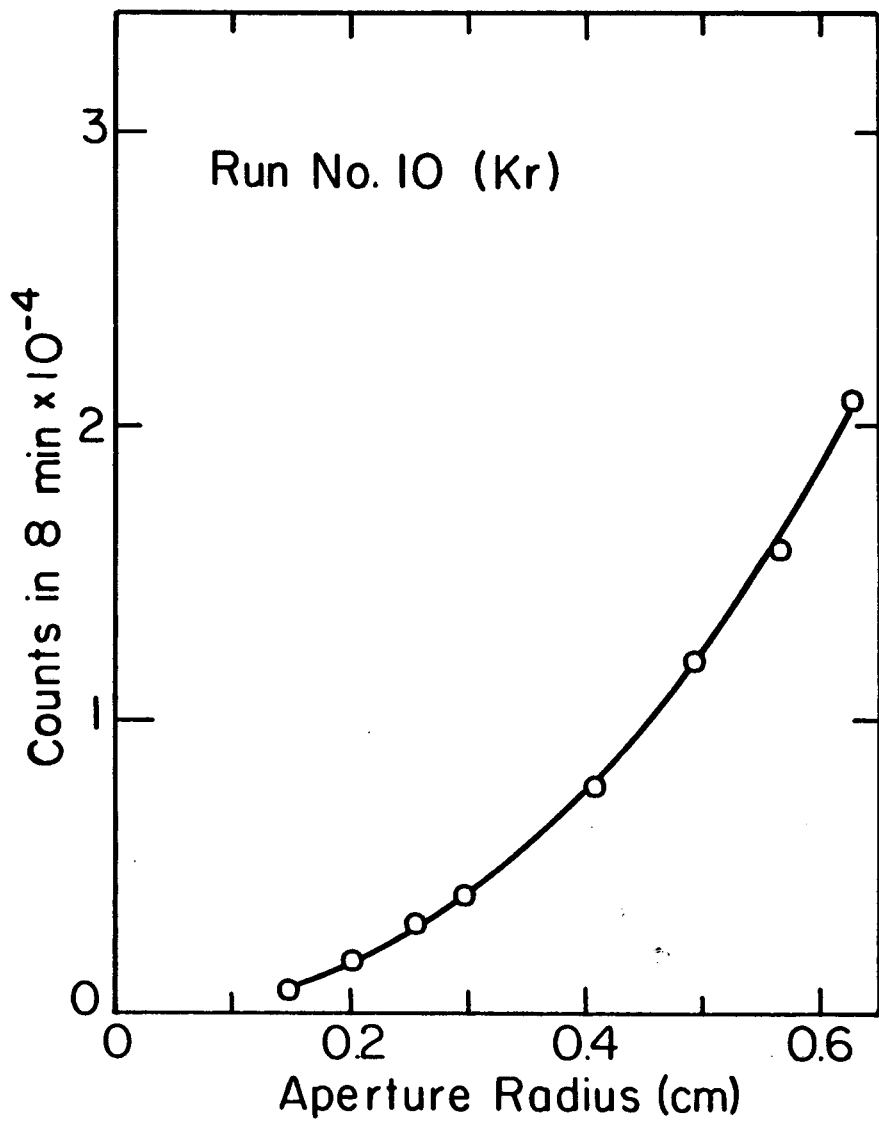
XBL 834-5491

Figure 4.



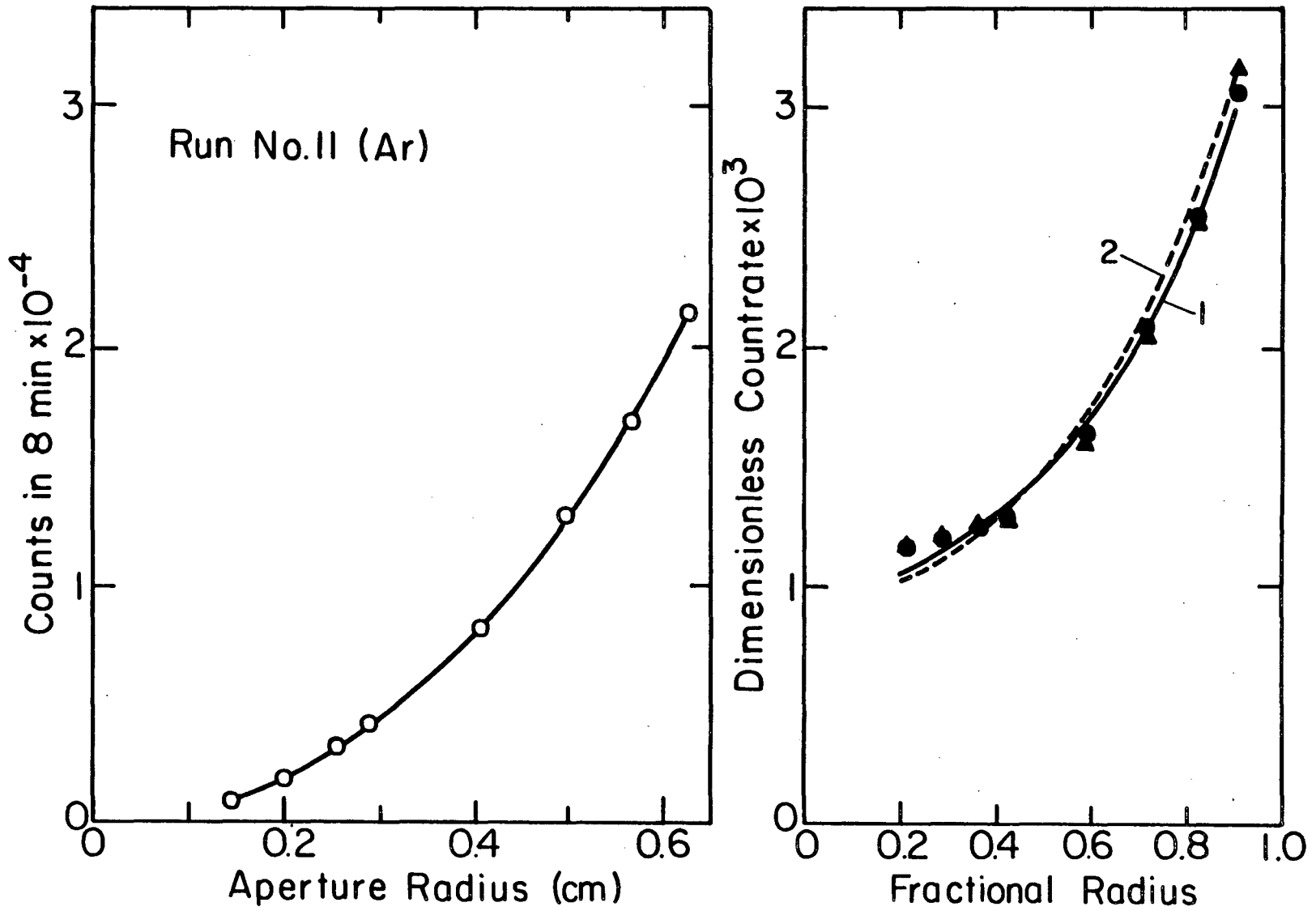
XBL 834-5492

Figure 5.



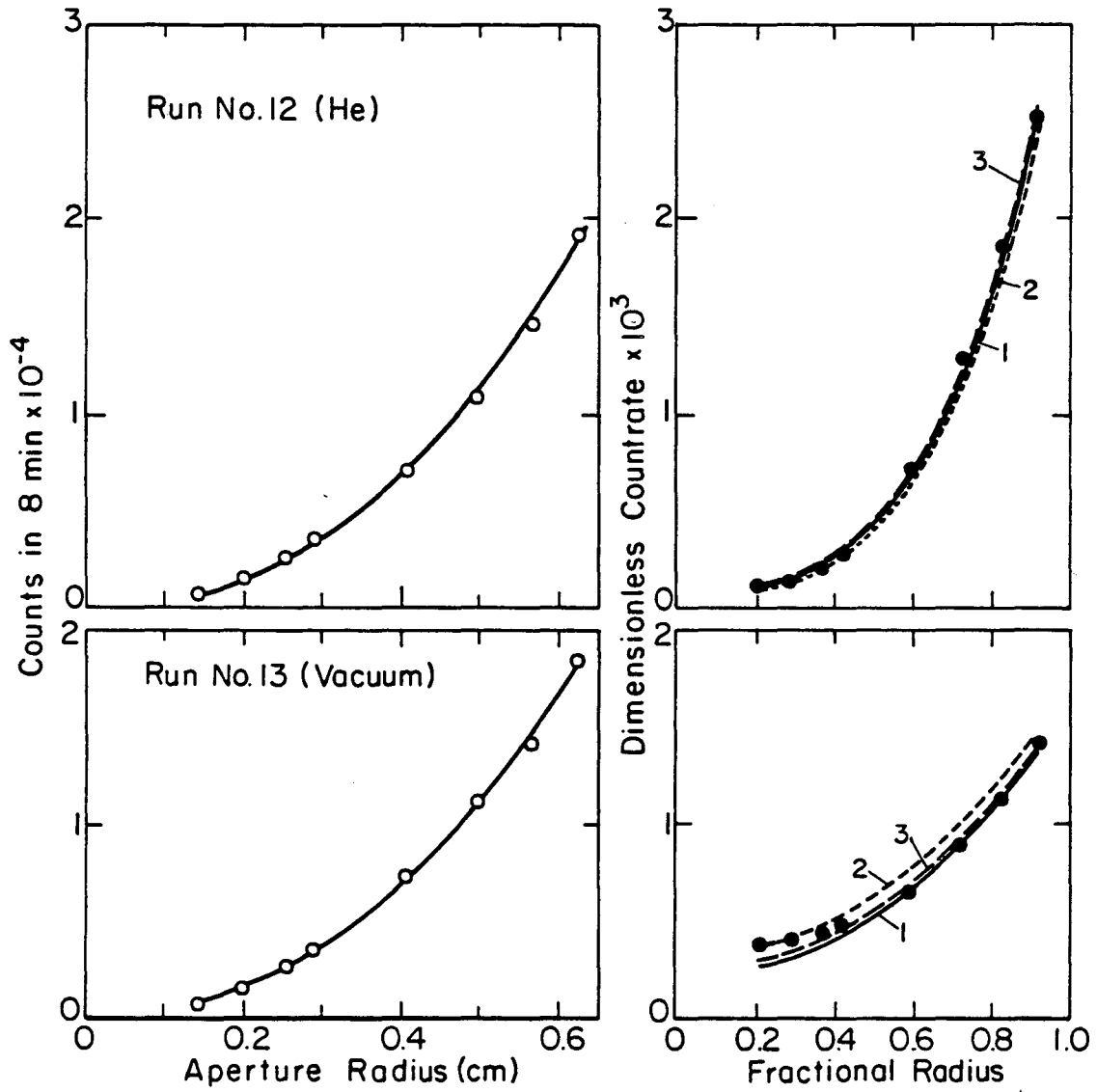
XBL 834-5493

Figure 6.



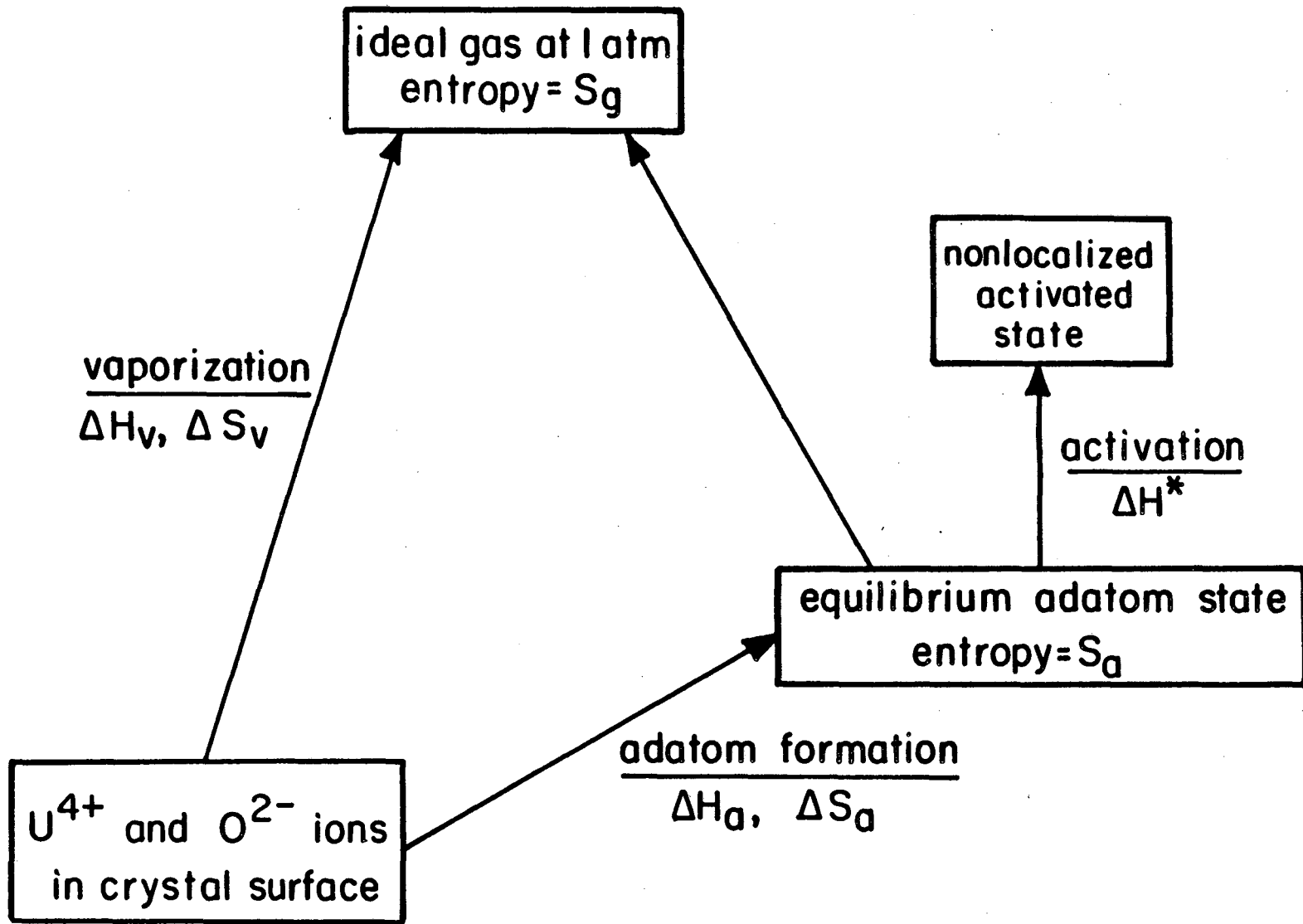
XBL 834-5494

Figure 7.



XBL 834-5495

Figure 8.



XBL 834-5506

Figure 9.

This report was done with support from the Department of Energy. Any conclusions or opinions expressed in this report represent solely those of the author(s) and not necessarily those of The Regents of the University of California, the Lawrence Berkeley Laboratory or the Department of Energy.

Reference to a company or product name does not imply approval or recommendation of the product by the University of California or the U.S. Department of Energy to the exclusion of others that may be suitable.

TECHNICAL INFORMATION DEPARTMENT
LAWRENCE BERKELEY LABORATORY
UNIVERSITY OF CALIFORNIA
BERKELEY, CALIFORNIA 94720